Molecular Plant Pathology

Dissecting the multifunctional role of the N-terminal disordered domain of the Melon necrotic spot virus coat protein in RNA packaging, viral movement and interference with antiviral plant defense.

Journal:	*Molecular Plant Pathology*
Manuscript ID	Draft
Manuscript Type:	Original Article
Date Submitted by the Author:	n/a
Complete List of Authors:	Serra-Soriano, Marta ; IBMCP (UPV-CSIC), PlantMolecular Virology Navarro, Jose ; IBMCP (UPV-CSIC), Plant Molecular Virology Pallas, Vicente; IBMCP (UPV-CSIC), Plant Molecular Virology
Keywords:	encapsidation, RNA-binding, silencing, Tombusvirus, siRNAs, Plant viruses

Dissecting the multifunctional role of the N-terminal disordered domain of the Melon necrotic spot virus coat protein in RNA packaging, viral movement and interference with antiviral plant defense.

Marta Serra-Soriano †, José Antonio Navarro*,† and Vicente Pallás*

Instituto de Biología Molecular y Celular de Plantas, IBMCP (Universitat Politècnica de València-Consejo Superior de Investigaciones Científicas), Ingeniero Fausto Elio s/n, 46022, Valencia, Spain.

† Marta Serra Soriano and José Antonio Navarro contributed equally to this work

*Correspondence Email: José Antonio Navarro, janavarr@ibmcp.upv.es and Vicente Pallás, vpallas@ibmcp.upv.es.

Correspondence Adress: Instituto de Biología Molecular y Celular de Plantas, IBMCP (Universitat Politècnica de València-Consejo Superior de Investigaciones Científicas), Ingeniero Fausto Elio s/n, 46022, Valencia, Spain. Phone: 0034963877877 Fax: 0034963877859

Running title: CP MNSV Nt-domain role in viral biology

Keywords: Plant viruses, siRNAs, encapsidation, RNA-binding, silencing, Tombusvirus.

Word counting: 6825

SUMMARY

To survive under high mutation rates, RNA plant viruses have evolved small genome sizes that strongly constrain the gain of function by gene duplication or lateral gene transfer. Very often, the solution to this pressure consists on the acquirement of new activities by viral proteins such as coat proteins (CP) already performing other roles in virus biology. Here, we showed that the R domain of *Melon necrotic spot virus* (MNSV) CP was crucial for CP multifunctionality. *in vitro* RNA binding kinetics revealed that deletion of the R domain abolishes RNA binding capability while, compared with wild-type, the apparent dissociation constant of partial deletion mutants increased. A conserved region between amino acids 60 and 91 appeared to play an essential role in *in vitro* RNA binding, but also in encapsidation of viral RNAs. However, the R domain integrity was indispensable for full-length genome assembly. In encapsidation-independent assays, we found that the R domain region from position 31 to 91, which included the above conserved region, was essential for efficient cell-to-cell movement. Interestingly, the same region was responsible for enhanced PVX pathogenicity, suppression of systemic RNA silencing and binding to small RNAs of 21, 22 and 24 nt. These findings indicate that, unlike other carmovirus CPs, the R domain of MNSV CP has evolved to acquire, in addition to other essential functions such as genome binding and encapsidation, the capability to suppress RNA silencing by preventing systemic small RNAs translocation.

INTRODUCTION

RNA virus populations are extremely vulnerable to a slight increase in deleterious mutations since RNA genomes replicate at or very close to the so-called error threshold (Elena and Sanjuan, 2005). To decrease lethality, plant RNA viruses have evolved to reduce their coding capacity and minimize genome size but still being competent pathogens (Belshaw *et al.*, 2007). This successful outcome comes from the fact that almost every viral protein has co-evolved with host plant to assume a wide array of structural and functional tasks. The viral coat proteins (CP), the main components of nucleocapsid shells, are not exceptions because they have roles in practically every step of viral biology, including genome replication, interference with plant antiviral defense, local and systemic movement and vector transmission (Callaway *et al.*, 2001).

Virions of *Melon necrotic spot virus* (MNSV), a member of the genus *Carmovirus* in the *Tombusviridae* family, are comprised of small spherical protein shells (30-nm-diameter) that encapsidate positive sense, monopartite, single-stranded RNA genomes of approximately 4.3 kb (Hibi and Furuki, 1985). Although MNSV genome shows the typical genome arrangement found in *Carmovirus* genus (Riviere and Rochon, 1990), similarities of its CP which those of *Tombusvirus* genus can be extended from primary to higher levels of protein structure (Riviere *et al.*, 1989; Wada *et al.*, 2008). Quaternary organization of MNSV capsids follows a T=3 icosahedral symmetry with 180 copies of three conformational quasi-equivalent CP subunits (A, B and C). Regardless of which type of subunit is considered, the tertiary structure of MNSV CP is composed of three major domains (Fig. 1). The middle S domain that builds a robust protein shell around the genome and the C-terminal P domain that projects outward from the capsid as dimers between adjacent subunits (30 C-C and 60 A-B dyads), have been found to adopt an ordered conformation in tombusviruses, carmoviruses and dianthoviruses (Doan *et al.*, 2003; Harrison *et al.*, 1978; Hogle *et al.*, 1986; Ke *et al.*, 2004; Morgunova *et al.*, 1994; Sherman *et al.*, 2006). The third domain of the MNSV CP or R-domain consisted of an N-terminal flexible arm of 94 residues that, in A- and B-type subunits, hangs down inside of the viral particle in a disordered way. Its basic nature along with its inner position makes evident that R domain must play an important role in genome binding during encapsidation (Rao, 2006). Otherwise, residues between Asn60 and Gly94 form an ordered arm in C-type subunits which extends from the inner face of the S-domain to icosahedral threefold

axes (Fig. 1). Three of such extended arms, each one projected from different C-C dyads, can be connected by hydrogen bonding around threefold axes to form a circular structure called β-annulus that provide additional stability to the viral particles (Pappachan *et al.*, 2008; Satheshkumar *et al.*, 2005).

Obviously MNSV CP plays also non-structural roles during infection. It enhances viral local spread most likely by interfering with post-transcriptional RNA silencing mechanisms (Genovés *et al.*, 2006) and mediates virion attachment to the surface of *Olpidium bornovanus* zoospores to be transmitted externally (Mochizuki *et al.*, 2008; Ohki *et al.*, 2010). The P domain was proved to be involved in compatibility with the fungal vector, but no other studies that relate further structural CP regions such as R domain to different functions, for example, virion assembly and suppression of RNA silencing have been reported until now. Taking into account this background, the present study was designed to explore the role of the R domain of MNSV CP in RNA binding and how this capability can modulate different steps of the viral biology. The MNSV CP affinity for long and small RNAs and that of a series of deletion and point mutations within the R domain was determined *in vitro*. The resulting mutants were also examined for their competence in viral RNA package, local spread, systemic movement and interference with antiviral RNA silencing. Our results demonstrated that R domain is highly essential for CP multifunctionality and survival of icosahedral plant viruses.

RESULTS

Mutations in the R domain affect *in vitro* RNA-binding properties of MNSV CP. Here, we follow the terminology of Wada *et al.* (2008) which defined the R domain of MNSV CP as the region comprised between positions 1 and 94. Thus, it also includes the so-called arm region that in C-type subunits is made by the β-annulus structure and ε region (Fig. 1) (Hui and Rochon, 2006).

Electrophoretic mobility shift assays (EMSA) were first conducted to estimate the ability of the wild type MNSV CP (CP(wt)) to bind RNA in solution. To avoid denaturing conditions during protein purification we were forced to use the GST-CP fusion. A constant amount of a viral RNA transcript (see experimental procedures) was incubated with increasing quantities of CP(wt). First panel in Fig. 2 shows a representative shift gel where the disappearance of the free RNA band was evident upwards of 10 ng of protein, indicating the formation of a protein-RNA complex. However, the resulting complex barely entered the matrix gel and, consequently, it was hardly transferred to the nylon membrane from the bottom of gel wells. In this situation, RNA-protein complex formation was measured as the disappearance of the band corresponding to unbound RNA (Marcos *et al.*, 1999). A Hill transformation was applied to data to plot the log [(1-x)/x] versus the log[CP(wt)], where x is [RNA]unbound/[RNA]total. The apparent dissociation constant (K_a) was calculated from the linear regression of the mean values from at least three independent experiments (Fig. S1) (Marcos *et al.*, 1999). K_a of CP(wt) was estimated to be 0.92 nM which is in the same order of magnitude of those calculated for some viral CPs (Aparicio *et al.*, 2003; Jansen *et al.*, 1998) but considerably lower than others (Baer *et al.*, 1994; Skuzeski and Morris, 1995). Shift gels with five different sense RNA transcripts covering MNSV full-genome indicated that CP(wt) did not preferentially recognize a particular nucleotide sequence (data not shown).

To elucidate the role of R domain in RNA binding, the amino acids at positions 1 to 91 were deleted in CP(ΔR) mutant leading to loss of interaction even at a high protein concentration (Fig. 2). To further identify the regions of R domain involved in such interaction, we defined three different R subdomains, each comprised of 30 residues with 5-6 positive charges (R_1,R_2 and R_3). Next, we engineered a series of mutations in which one or two of these subdomains were deleted (Fig 1). None of the subdomain deletions rendered MNSV CP incompetent for RNA binding,

although affinity was always weakened (Fig. 2 and S1). The highest detrimental effect was observed in CP($\Delta R_{2,3}$), CP($\Delta R_{1,3}$) and CP($\Delta R_{1,2}$) mutants, all of them harboring two subdomains deletion. Regardless of which subdomain was present in these mutants, their K_{as} were comparable and estimated to be between 139 and 196 times higher than in CP(wt). K_a of CP(ΔR_1) or CP(ΔR_2) was only 3.5 or 8.4 times higher than in CP(wt), respectively. In contrast, deletion of R_3 subdomain in CP(ΔR_3) had a much drastic effect increasing the K_a up to 70 times that of CP(wt) (Fig. 2). From this data, it is apparent that R_3 subdomain plays an important role in *in vitro* RNA binding which is facilitated by the presence of upstream residues either from R_1 or R_2 subdomains.

The ε region contains most of the basic residues within R_3 subdomain (Fig. S2). To establish their contribution in RNA binding, mutations to Ala were introduced in four of the positively charged residues of the ε region most exposed to the protein surface. All mutations had negative effects on protein-RNA binding, but they were significantly different depending on each mutant. CP(R91A), which affects a low conserved Arg (Fig. S2), leads to a slightly 4-fold reduction in RNA affinity (K_a=3.76 nM). Interestingly, single substitution of MNSV-specific Arg81 (CP(R81A)) had a more severe impact on RNA binding (K_a=54.5 nM) than mutations in fully conserved Lys86 (CP(K86A) and Arg88 (CP(R88A) (K_a=7.19 nM and 5.96 nM, respectively). Remarkably, K_a of CP(R81A) was 54.5 nM, which is in the same order of magnitude to that of CP(ΔR_3) indicating that Arg81 has a relevant participation in RNA binding.

The full-length R domain is required for encapsidation of genomic RNA. To know whether R domain mutations affect *in vivo* packaging of viral RNAs, CP(wt), R subdomains deletion mutants, CP(ΔR) and CP(R81A) ORFs (Fig. 1) were cloned into a MNSV infectious binary vector (Fig 3A). Agroinfiltration of cotyledons, which accumulate higher quantities of virions than leaves (Serra-Soriano *et al.*, 2015), was used as a sensitive and cell-to-cell movement independent assay. All mutants were found to produce viral or viral-like particles (VLP) dense enough to reach the bottom of a 20 % sucrose cushion as revealed by dot-blot immunodetection (Fig. 3B). CP titer of purified particles was measured by serial dilution and, in the majority of mutants, signal intensities were reduced in more than 100-fold that of wild-type, indicating that any modification of the R domain greatly decreased viral particle production. Next, capability of viral RNA packaging was determined by Northern blot analysis. Equal amounts of viral particles, which

were estimated by dot-blot immunodetection, were subjected to agarose gel electrophoresis in native conditions to preserve virion structure. Only mutants harboring CP($\Delta R_{1,2}$), CP(ΔR_2), CP(ΔR_1) or CP(R81A) mutations were able to encapsidated viral RNAs. However, all four yielded hybridization signal intensities lower than that obtained in wild-type infection, suggesting that RNA package into virions was significantly reduced (Fig. 3C). Northern blot analysis of total RNAs showed that all mutants accumulate both genomic (gRNA) and subgenomic (sgRNA) RNAs at levels comparable or higher than that of wild type (Fig. 3D). This observation demonstrates that the results obtained before are not primary due to a deficiency in viral RNAs accumulation in infected tissue. However, northern blot analysis of RNAs extracted from particles produced by CP($\Delta R_{1,2}$), CP(ΔR_2), CP(ΔR_1), CP(R81A) and CP(wt) only showed detectable levels of full-length genomic RNA in the case of CP(R81A) and CP(wt) (Fig. 3E). Three viral RNA species smaller than MNSV genome were also observed. The two lower molecular weight species likely correspond to both MNSV sgRNAs (1.9 and 1.6 kb). The biggest RNA (approximately 2 kb) may represent a defective interfering RNA (DI RNA) or could it simply be the result of gRNA degradation.

Interestingly, all competent mutants for RNA encapsidation maintained the R_3 subdomain that was previously shown to play an essential role in in vitro RNA binding. Although CP(R81A) mutation had less effect on viral RNA package into virions than expected, these findings are in high correlation with *in vitro* results.

The R domain of MNSV CP modulates cell-to-cell movement independently of its role in encapsidation. We previously demonstrated that RNA encapsidation was not a prerequisite for MNSV cell-to-cell movement since local spread was decreased but not inhibited when the CP gene was replaced by GFP. We also showed that transport efficiency was recovered when either MNSV CP or a heterologous viral suppressor of RNA silencing (VSR) was provided *in trans* suggesting a role for MNSV CP in eluding host defense (Genovés *et al*., 2006). Here, to compare the ability of R domain mutants to move from cell to cell with that of wild type, each CP variant was introduced into a MNSV binary vector that take advantage of the TaV 2A catalytic peptide to express both GFP and CP genes under the same viral promoter (Fig. 4A) (Serra-Soriano *et al.*, 2014). This viral RNA resulted to be not competent for packaging most likely due to its recombinant genome is larger than native genome, a situation that has been reported for the related carmovirus *Turnip crinkle*

virus (TCV) (Qu and Morris, 1997). Since viruses harboring R domain deletion mutants appear not to encapsidate full-length genome, that construct allows us to compare the movement of the wild-type and mutant variants under equal non-encapsidation conditions.

Cell-to-cell movement was monitored at 6 and 12 days post-infiltration (dpi) by measuring the area of fluorescent infection foci in six fully expanded melon leaves per mutant. Each bar diagram in Fig. 4B represents the average of foci size means from three independent experiments (approximately 600 foci per mutant). At 6 dpi, the wild-type virus induced fluorescent foci of 0.230±0.006 mm^2 on average size; in contrast, movement was significantly (*p* value <0.0001) reduced in almost all mutants which formed infection foci showing mean sizes ranging from 0,091±0,015 to 0.146±0.017 mm^2. Only mutant harboring CP(ΔR_1) mutation produced foci significantly (p<0.0001) higher than those of wild-type (0.333±0.035 mm^2). At 12 dpi the situation was similar, wild-type and CP(ΔR_1) mutant infections progressed to reach infection foci sizes 5-fold higher than before (1.24±0.02 and 1.75±0.19 mm^2, respectively). The rest of mutants showed infection foci smaller than those of wild-type (Fig. 4B and 4C). Statistical analysis indicated that the mean area of the infection foci formed by these mutants were significantly different from that of the wild-type (p≤0.0008) except for CP(R81A) mutant (p=0.53) (1.24±0.02 vs 1.13±0.03 mm^2). Similarly to RNA binding results obtained before, single deletion mutants harboring R_3 subdomain and CP(R81A) mutant had also the smallest deleterious effect on cell-to-cell movement.

Enhanced pathogenicity and increased viral RNA accumulation in PVX infections after expression of MNSV CP is dependent on the R domain region between amino acids 31-91. We next wanted to reevaluate the VSR activity of MNSV CP using an assay based on enhanced *Potato virus X* (PVX) pathogenicity when an additional VSR is provided *in cis* (Voinnet *et al.*, 1999). We also assessed the relevance of the R domain, and especially that of the R_2 and R_3 subdomains, in MNSV CP silencing suppression phenotype. We hence introduced the coding sequences of wild-type MNSV CP and mutated CP(ΔR_1), CP(ΔR_2), CP(ΔR_3), CP(ΔR) and CP(R81A) into a PVX-derived binary vector (Lacomme and Chapman, 2008). PVX-permissive host *N. benthamiana* was agroinfiltrated and three weeks later, plants were imaged (Fig. 6A). Those plants infected with PVX that expressed either wild-type MNSV CP (PVX-CP(wt)) or mutated

CP(ΔR_1) (PVX-CP(ΔR1)) showed severe stunting and necrosis (Fig. 5A). In contrast, phenotype of plants infected with PVX-CP(ΔR) was more comparable to that of control infections with empty PVX. In both cases infected plants only displayed mild symptoms that progressively disappeared in upper leaves. Plants infected either with PVX-CP(ΔR_2) or PVX-CP(ΔR_3) showed a slightly more severe symptomatology than PVX-CP(ΔR) and finally, plants infected with PVX-CP(R81A) had increased symptomatology but without reaching the severity observed in PVX-CP(wt) and PVX-CP(ΔR1). Total RNAs from non-agroinfiltrated leaves were also analyzed by Northern blot with a PVX CP specific riboprobe (Fig. 5B). Hybridization signals revealed substantially more accumulation of viral RNAs in plants infected either with PVX-CP(wt) or PVX-CP(ΔR1) than in those infected with control PVX and with each of the PVX variants examined. Therefore, VSR function is dependent on R domain and, specifically, on the region embracing both R_2 and R_3 subdomains

MNSV CP binds Dicer-like small RNAs through the R domain region between amino acids 31-91.

To study MNSV CP binding to small RNAs, we performed gel shift assays and kinetic analysis essentially as hereinbefore described. We first used MNSV CP(wt) and *in vitro* transcripts either of 21, 22 or 24 nt to determine the optimal protein concentration at which to perform further comparisons with R domain mutants. Increasing quantities of GST-CP(wt) lowered the amount of free single stranded RNAs (ssRNAs) independently of its size and resulted in the formation of ssRNA-CP complexes that, as occurred before, barely enter the gel (Fig. 6A). Disappearance of free ssRNAs of 21 and 22 nt began to be more evident at higher protein concentrations than in the case of ssRNAs of 24 nt. This observation was reflected in the values of the corresponding apparent dissociation constants (Fig 6B). K_{as} for the binding of MNSV CP to 21 and 22 nt ssRNAs were similar and it was estimated to be 180 nM. In contrast, a four-fold increase of affinity for the binding of MNSV CP to 24nt sRNAs was found (K_a, 50 nM). These results may indicate that MNSV CP binds ssRNAs in a size-selective manner, and suggest a preference for 24 nt ssRNAs.

To examine whether the loss of silencing suppressor activity coincides with loss of binding affinity to siRNA molecules, GST-recombinant R domain mutants were compared with GST-CP(wt) in gel mobility shift assays. Next experiments were performed using a single protein concentration.

Therefore, to avoid misinterpretations of binding specificity (Ryder *et al.*, 2008) and to guarantee that complex formation was not limited by protein availability, we used a concentration (600 nM) at which unbound RNA practically disappeared in the assays performed above. ssRNAs of 21, 22 and 24 nt but also the corresponding RNAs duplexes (dsRNAs) containing 2-nt 3' end overhangs were incubated with CP(wt) and R domain mutants (Fig. 7A and 7B, respectively). EMSAs revealed that only CP(wt) and CP(ΔR1) showed binding activity to single and double stranded RNAs of 21, 22 and 24 nt, whereas the rest of mutants failed to form complexes with either type of RNA tested (Fig. 4B). These results indicate that the R domain region between amino acid 31-91 is required for silencing suppression and binding of siRNAs and, consequently, corroborate our initial assumption that both properties should be closely linked.

MNSV CP inhibition of systemic RNA silencing triggered by sense GFP RNA is also dependent on the R domain region between amino acids 31-91. When RNA silencing was triggered by sense GFP RNA using GFP transgenic *N. benthamiana* plants (line 16c), MNSV CP exhibited a weak suppressor activity of transgene silencing in local infiltrated leaves (Genovés et al., 2006). However, effects on upper non-infiltrated leaves were not examined. To determine whether MNSV CP could interfere with systemic RNA silencing, five 16c plants were infiltrated with a mix of two *A. tumefaciens* cultures either expressing GFP or CP(wt). Bacteria carrying binary vectors either expressing each R domain deletion mutant, CP(R81A) mutant or an unrelated protein, which was used as positive control for systemic silencing, were also included into the assay. Three independent experiments were performed. Development of GFP systemic silencing was monitored, under UV light, following the appearance and spread of red chlorophyll autofluorescence. In all control plants, the upper noninfiltrated leaves started to lose green GFP fluorescence around major veins at approximately 10-12 dpi. At 25-30 dpi, the whole plant lost green fluorescence and became completely red under UV light (Fig. 8). Almost all plants (around 90%) coinfiltrated with GFP plus CP(wt) or GFP plus CP(ΔR_1) retained green fluorescence in noninfiltrated leaves at 30 dpi. In contrast, plants infiltrated with GFP plus either of remaining seven mutants behaved similarly to control plants (Fig. 8). None of the analyses described at present has been conclusive about molecular form of the mobile RNA that triggers systemic silencing but

siRNAs have become the most plausible option. These results are in line with those obtained in siRNA binding experiments indicating that MNSV CP could suppress systemic RNA silencing by small RNA sequestering.

DISCUSSION

In this work, we have examined the N-terminal region or R domain of MNSV CP for its relevance in multiple and essential processes in the viral life cycle. We showed that MNSV CP binds with high affinity to long viral ssRNAs without detectable sequence specificity. We also demonstrated that RNA binding exclusively depends on the R domain since RNA interaction was completely eliminated after deletion of the very 94 N-terminal amino acid residues. Although there were significant variations between RNA affinities among the rest of R domain mutants, they were proved to be insufficient to abolish *in vitro* RNA binding ability. This indicates that, at least in solution, all 16 basic residues located along the R domain can potentially contribute to interact with negatively charged RNA backbones. However, the presence of the R_3 subdomain appeared to be more relevant in single than in double subdomain deletion mutants since the deletion of this subdomain had a significantly stronger effect in the RNA-binding affinity than the deletion of either R_1 or R_2 subdomains.

Consistently with these results, the presence of R_3 subdomain was proven to be required for RNA encapsidation during plant infection. Neutron diffraction studies on *Tomato bushy stunt virus* (TBSV) and cryo-transmission electron microscopy structures of *Cucumber necrosis virus* (CNV) revealed that tombusvirus particles were internally organized in four alternating concentric shells of protein and RNA (Katpally *et al.*, 2007; Timmins *et al.*, 1994). The outer protein shell corresponded to the S and P domains while the second internal protein shell was formed by most of disordered N-terminal region. Most of viral RNA was very tightly packed between both protein shells, showing higher density under C-C dyads than under A-B dyads. In contrast, RNA density was lacking close to the highly hydrophobic β-annulus elements at the threefold axis. High structural homology among MNSV and TBSV CPs has been reported (Wada *et al*., 2008). In fact, the ε region of MNSV CP is also highly basic, containing five positively charged residues, while only a basic residue is found in the β-annulus sequence. This led us to assume that MNSV capsid may display a TBSV-like internal architecture and similar distribution of the RNA density under the inner surface of the

outer protein shell, supporting the major role of the ε region within the R_3 subdomain in MNSV RNA encapsidation.

It has been shown that removal of an extended N-terminal region facilitates CP to assemble into 60 subunits T=1 particles that are significantly smaller than the native T=3 particles (Hsu *et al.*, 2006; Kakani *et al.*, 2008; Katpally et al., 2007; Kumar *et al.*, 1997; Larson *et al.*, 2005; Sangita *et al.*, 2004). Thus, deletion of R_1, R_2 or both subdomain could modify T=3 symmetry of MNSV virions, resulting in smaller capsids large enough to ensure encapsidation of sgRNAs but not full-length genomes. This assumption could explain why MNSV RNAs of approximately 4.3 kb were only recovered from wild-type and CP(R81A) mutant virions, which have the complete R domain, but not from other deletion mutants. In this sense, recombinant TCV RNAs larger than parental genomes were unsuccessfully encapsidated (Dong *et al.*, 1998). As another possible explanation, N-terminal deletions could compromise inner shell formation affecting morphology and/or stability of viral particles. Without ruling out the possibility that inner shell can be also required in recognition of MNSV RNAs as observed in EMSAs, unsuccessful encapsidation of full-length genome could result from an increased accessibility of nucleases inside the unstable mutant particles, as previously proposed for CNV (Reade *et al.*, 2010).

We previously showed that the potential role of MNSV CP as VSR was barely demonstrated by a standard bioassay on transgenic 16c *N. benthamiana* (Genovés *et al.*, 2006). The results obtained here indicate that MNSV CP suppression of viral induced silencing, which has biological significance for viral infection, seems to be more evident than suppression of transgene induced silencing. Similar discrepancy has been already reported for others VSRs and it is most likely due to the fact that PVX assay more closely mimics wild-type conditions produced by cytoplasmic RNA viruses (Powers *et al.*, 2008). The link between the VSR activity and their effects on the pathogenic process has been well documented (see García and Pallás, 2015 for a review). Here we demonstrated that VSR function is dependent on R domain and, specifically, on the region embracing residues from 30 to 91. In encapsidation independent movement assays, only CP(ΔR1) mutant showed a phenotype similar to that observed in wild-type infections. Therefore, the same region of MNSV R domain required for VSR activity was essential for efficient viral movement,

indicating that defects in combating the host defense system are likely causing restrictions in cell-to-cell movement.

Interestingly, deletion of the R_1 subdomain significantly increased cell-to-cell movement. In CNV, the N-terminal 39 amino acids of the CP can function as a mitochondrial targeting peptide (mTP) resulting in a proteolytic cleavage of the R domain near the R/arm junction (equivalent to the R_2/R_3 subdomain junction in MNSV) (Hui *et al.*, 2010). These researchers proposed that mitochondrial targeting of CNV CP could determine its destiny towards assembly or disassembly during infection. We have also experimental evidences that dual targeting to mitochondria and chloroplast followed by proteolytic cleavage of the R domain occurs in MNSV CP(wt) but not in CP(ΔR1) mutant (unpublished results). Although more studies are required, CP(wt) suppressor activity could be compromised in CP(wt) by proteolytic cleavage but not in CP(ΔR1) mutant. Thereby, more CP(ΔR1) protein could be fated to act as VSR facilitating local spread.

Two observations made us to speculate that binding siRNAs could be the molecular mechanism by which MNSV CP interferes with RNA silencing: first, viral-derived siRNAs, mainly of 21 nt, accumulated to abundant levels in infected plants, suggesting that MNSV CP does not prevent siRNA production *in vivo* (Donaire *et al.*, 2009; Herranz *et al.*, 2015); second, we demonstrated here that suppressor activity of MNSV CP *in vivo* was dependent on basic R domain. Shift mobility gels showed that purified MNSV CP can bind DICER-like sRNAs *in vitro* independently of their size. Moreover, our mutational analysis revealed a positive correlation between the ability to bind sRNAs *in vitro* and the capacity to suppress RNA silencing *in vivo*, strongly indicating that MNSV CP interfere with viral RNA degradation by sequestering sRNAs. It has been shown that 24 nt rather than 21 nt sRNAs were selectively mobile through the systemic pathway, at least from a GFP transgene and from selected endogenous loci (Melnyk *et al.*, 2011). Our results demonstrated that MNSV CP showed higher affinity for sRNAs of 24 nt, a functional feature that could be involved in blocking the spread of the mobile systemic signal of RNA silencing (Cao *et al.*, 2010; Zhang and Simon, 2003).

Tough MNSV belongs to genus *Carmovirus*, its CP is more similar to those of genus *Tombusvirus* in the extent of sequence similarity, length of the R and P domains and tridimensional

structure (Wada *et al*., 2008; Riviere *et al*., 1989). These findings indicate that MNSV CP gene could have been acquired during a recombinant process. In this regard, tombusviruses and carmoviruses have been predicted to be highly recombinant compared to viruses of the other genera in *Tombusviridae* family (Boulila, 2011). Moreover, recombination may occur between viruses belonging to different genera and particularly in the coat protein-encoding gene (Boulila, 2011). Such a recombinant event was largely studied for CNV and MNSV (Riviere and Rochon, 1990). In the family *Tombusviridae*, CPs of carmoviruses and P19 protein, which is entirely nested within the movement protein of tombusviruses, have been described as major suppressors of RNA silencing (Burgyan and Havelda, 2011). In contrast, CPs of tombusvirus are lacking of VSR activity. In fact, MNSV CP lacks the GW motif that is present in carmovirus CPs and in the only member of the recently proposed *Pelarspovirus* genus (Azevedo *et al.*, 2010, Pérez-Cañamás and Hernández, 2015). The GW motif mimics the GW/WG repetitive motif of cellular AGO interacting proteins and, in the case of TCV CP, it has been proposed to avoid sRNA loading into AGO1 by interacting with nonloaded AGO1. In addition to this protein-protein interaction, carmovirus CPs have been postulated to bind viral sRNAs as an alternative mechanism of RNA silencing (Merai *et al.*, 2006). This binding relies on specific basic amino acids within the S domain of the CP (Cao *et al*., 2010). Our results demonstrate the peculiarity of the MNSV CP in its mode of action for its RNA silencing activity. Moreover, the relevance of GW motif in sRNA binding has been also demonstrated (Azevedo *et al*., 2010, Pérez-Cañamás and Hernández, 2015). In the absence of P19-like proteins or *bona fide* carmovirus CP, MNSV CP could have acquired VSR activity by adapting its N-terminal disordered region to interact with different RNA molecules such as siRNAs. As MNSV encapsidation and suppression functions rely on same functional domain of the CP, they should be mutually exclusive processes. Therefore, further studies are needed to identify the physiological or molecular switch that determines the fate of MNSV CP toward encapsidation or RNA silencing suppression.

EXPERIMENTAL PROCEDURES

Plasmid construction. For protein production in bacteria, MNSV CP gene was PCR-amplified from pMNSV(Al) (Genovés *et al*., 2006) and cloned into pGEX-KG (GE Healthcare Life Sciences) to generate pG-CP(wt). For making deletions, inverse PCR was employed using either pG-CP(wt)

or pG-CP(ΔR_1) as template and divergent 5'-phosphorylated primers (Table S1). The resulting fragments were circularized by self-ligation. Point-mutations were introduced by site-directed mutagenesis using the QuickChange XLSite-Direct Mutagenesis Kit following manufacturer's instructions (Agilent Technologies) and primers listed in Table S1.

To make binary vectors harboring either CP(wt) or each CP mutant, the full-length genome of MNSV was amplified from pMNSV(Al) and cloned between the CaMV 35S promoter and PoPit terminator into a modified pBSIIKS(+) (Agilent Technologies). The resulting p35-MNSV(Al) plasmid was the basis to introduce all CP deletions and R81A point-mutation as was done before for pGEX. Next, each expression cassette was amplified using M13 forward and reverse primers and cloned into pMOG800 binary vector (Knoester *et al.*, 1998).

To measure the cell-to-cell movement extent, the previously constructed p35-MNSV(Al)/GFP vector was used (Serra-Soriano *et al.*, 2014). MNSV(Al)/GFP RNA express both GFP and CP from a bicistronic gene (GFP-CP) which product is processed during translation by means of the self-cleaving 2A peptide of *Thosea asigna virus* (TaV). A cloning strategy relying on the use of BveI type IIs endonuclease was used to introduce all CP deletion mutants and R81A point-mutation (Table S1). Expression cassettes from all constructs were amplified as before and cloned into pMOG800.

MNSV CP(wt), deletion mutants and CP(R81A) mutant genes were also amplified using as template the constructs obtained before and cloned between the CaMV 35S promoter and PoPit in pMOG800. Moreover, PVX-derivatives containing the CP(wt), deletion mutants and R81A point-mutation were obtained by cloning the corresponding ORFs downstream of the duplicated PVX coat protein promoter in pGR107 (Jones *et al.*, 1999).

Protein expression and purification in bacteria. pGEX constructs were transformed into *E. coli* BL21(DE3) pLysS cells. Protein expression was induced at 18 °C for 14-16 h by IPTG addition and proteins purified under non-denaturing conditions by affinity chromatography with glutathione-Sepharose 4B as indicated by the manufacturer (GE Healthcare Life Sciences). Protein concentration was determined with the Bio-Rad protein assay reagent using a series of BSA standards and Tecan plate reader.

Nucleic acid binding assay. Protein-RNA binding studies were performed by means of electrophoretic mobility shift assay (EMSA) as previously described (Herranz and Pallás, 2004). Briefly, a constant amount (5 ng) of a digoxigenin-labelled RNA transcript, which include the nucleotide sequence comprised between the positions 2443 and 2828 of MNSV(Al), was incubated with increasing amounts of each recombinant protein. Samples were electrophoresed on a 1% agarose gel in 1X TAE and transferred to nylon membranes (Roche Diagnostic GmbH). Viral RNA detection was conducted using CSPD chemiluminescent substrate (Roche Diagnostic GmbH) as previously described (Pallás *et al.*, 1998). Band densitometry was performed using Luminescent Image Analyzer LAS-3000 and Fujifilm Multigauge 3.0 software (Fujifilm). EMSA for each recombinant protein was repeated between three and five times to ensure reproducibility and accurate linear regression (R-squared values higher than 0.9) of Hill transformation (Marcos et al., 1999). Wild type CP was always included as a control to address between-experiment variation. In some experiments, digoxigenin-labelled single- and double-stranded small RNAs (21, 22 and 24 nt long) were used in binding assays. Single-stranded small RNAs were obtained by *in vitro* transcription using double stranded DNA oligonucleotides (Table S1). Double-stranded RNA molecules containing two nucleotide overhangs on their 3' end were obtained by annealing equimolar mixtures of complementary single-stranded RNAs. Binding assay and densitometry were conducted as described above but samples were subjected to 5 % PAGE in 1X TAE and wet-transferred onto nylon membranes.

Virion purification assays. *Agrobacterium tumefaciens* strain C58C1 harboring each MNSV binary constructs were infiltrated into cotyledons of one-week-old melon plants. Two weeks later, 10 g of agroinfiltrated melon cotyledons per construct were homogenized in liquid nitrogen. A small quantity of the resulting powder (100 mg) was reserved for total RNA extraction with **TRIzol** Reagent while the rest of the homogenate was used for virion purification through a 20% sucrose cushion as previously described (Diez *et al.*, 1998). To determine the relative amounts of virions, 10-fold serial dilutions of all stocks were dotted onto PVDF membranes (GE Healthcare Life Sciences) and subsequently used for immunodetection with a polyclonal antibody against the MNSV (Loewe Biochemica). Next, equivalent quantities of virions were electrophoresed through 1 % agarose gel in TAE 1X and blotted overnight onto nylon membranes as described before. For

total RNA extracts, 2 µg of each sample were electrophoresed in denaturing 1.2 % agarose gel (3 % formaldehyde, 40 mM MOPS, 10 mM sodium acetate and 1 mM EDTA, pH 7.0). Viral RNA detection was performed by overnight hybridization as previously described (Pallás *et al*., 1998) using a digoxigenin labelled-riboprobe againts the 3' end region of the MNSV CP gene. The complete assay was repeated three times.

Cell-to-cell movement assay. Cell-to-cell movement was monitored as previously described by examining the formation of fluorescent foci (Navarro *et al.*, 2014; Serra-Soriano *et al*., 2014). The binary constructs were agroinfiltrated (OD_{600} of 0.2) into fully expanded leaves from 2-week-old melon plants. Three independent experiments were performed in which ten leaves from five plants per construct were used each time. Images of fluorescent infection foci were taken at 6 and 12 days post-infiltration using a Leica MZ12 fluorescent stereomicroscope (Leica microsystems). Infected areas were measured using FIJI free software (http://fiji.sc/Fiji) and data were analyzed using MS Excel (Microsoft). GraphPad Prism 6 software and Student's t-test (p value<0.05) was used to determine the statistical significance of results.

Assay for pathogenicity of *Potato virus X* derivatives in *N. benthamiana*. After electroporation, each of the construct was propagated in *A. tumefaciens* strain C58C1 containing the helper plasmid pSoup, grown to OD_{600} of 0.5, and infiltrated into *N. benthamiana* plants. Three weeks later, the plants were photographed and non-infiltrated leaves collected for total RNA extraction and Northern blot analysis. Viral RNA detection was performed by overnight hybridization with a 500 nt length digoxigenin labelled-riboprobe complementary to the 3' end region of the PVX CP gene. The experiment was repeated three times.

ACKNOWNLEDGMENTS

This work was funded by grant BIO2014-54862-R from the Spanish Direccion General de Investigacion Cientifica y Tecnica (DGICYT) and the Prometeo Program GV2014/010 from the Generalitat Valenciana. J.A.N. and M.S. are the recipients of a postdoctoral contract and a PhD fellowship from the Ministerio de Educacion y Ciencia of Spain. We thank L. Corachan for her technical assistance. The authors have no conflict of interest to declare.

REFERENCES

Aparicio, F., Vilar, M., Pérez-Payá, E. and Pallás, V. (2003) The coat protein of prunus necrotic ringspot virus specifically binds to and regulates the conformation of its genomic RNA. *Virology,* **313,** 213-223.

Azevedo, J., García, D., Pontier, D., Ohnesorge, S., Yu, A., García, S., Braun, L., Bergdoll, M., Hakimi, M.A., Lagrange, T. and Voinnet, O. (2010) Argonaute quenching and global changes in Dicer homeostasis caused by a pathogen-encoded GW repeat protein. *Genes Dev.* **24,** 904-915.

Baer, M.L., Houser, F., Loesch-Fries, L.S. and Gehrke, L. (1994) Specific RNA binding by amino-terminal peptides of alfalfa mosaic virus coat protein. *EMBO J.* **13,** 727-735.

Belshaw, R., Pybus, O.G. and Rambaut, A. (2007) The evolution of genome compression and genomic novelty in RNA viruses. *Genome Res.* **17,** 1496-1504.

Boulila, M. (2011) Positive selection, molecular recombination structure and phylogenetic reconstruction of members of the family Tombusviridae: Implication in virus taxonomy. *Genet. Mol. Biol.* **34,** 647-660.

Burgyan, J. and Havelda, Z. (2011) Viral suppressors of RNA silencing. *Trends Plant Sci.* **16,** 265-272.

Callaway, A., Giesman-Cookmeyer, D., Gillock, E.T., Sit, T.L. and Lommel, S.A. (2001) The multifunctional capsid proteins of plant RNA viruses. *Annu. Rev. Phytopathol.* **39,** 419-460.

Cao, M., Ye, X., Willie, K., Lin, J., Zhang, X., Redinbaugh, M.G., Simon, A.E., Morris, T.J. and Qu, F. (2010) The capsid protein of Turnip crinkle virus overcomes two separate defense barriers to facilitate systemic movement of the virus in Arabidopsis. *J. Virol.* **84,** 7793-7802.

Diez, J., Marcos, J.F. and Pallás, V. (1998) Carmovirus isolation and RNA extraction. *Methods Mol. Biol.* **81,** 211-217.

Doan, D.N., Lee, K.C., Laurinmaki, P., Butcher, S., Wong, S.M. and Dokland, T. (2003) Three-dimensional reconstruction of hibiscus chlorotic ringspot virus. *J. Struct. Biol.* **144,** 253-261.

Donaire, L., Wang, Y., Gonzalez-Ibeas, D., Mayer, K.F., Aranda, M.A. and Llave, C. (2009) Deep-sequencing of plant viral small RNAs reveals effective and widespread targeting of viral genomes. *Virology,* **392,** 203-214.

Dong, X.F., Natarajan, P., Tihova, M., Johnson, J.E. and Schneemann, A. (1998) Particle polymorphism caused by deletion of a peptide molecular switch in a quasiequivalent icosahedral virus. *J. Virol.* **72,** 6024-6033.

Elena, S.F. and Sanjuan, R. (2005) Adaptive value of high mutation rates of RNA viruses: separating causes from consequences. *J. Virol.* **79,** 11555-11558.

García, J.A. and Pallás, V. (2015) Viral factors involved in plant pathogenesis. *Curr. Opin. Virol.* **11,** 21-30.

Genovés, A., Navarro, J.A. and Pallás, V. (2006) Functional analysis of the five melon necrotic spot virus genome-encoded proteins. *J. Gen. Virol.* **87,** 2371-2380.

Harrison, S.C., Olson, A.J., Schutt, C.E., Winkler, F.K. and Bricogne, G. (1978) Tomato bushy stunt virus at 2.9 A resolution. *Nature,* **276,** 368-373.

Herranz, M.C., Navarro, J.A., Sommen, E. and Pallás, V. (2015) Comparative analysis among the small RNA populations of source, sink and conductive tissues in two different plant-virus pathosystems. *BMC Genomics,* **16,** 117.

Herranz, M.C. and Pallás, V. (2004) RNA-binding properties and mapping of the RNA-binding domain from the movement protein of Prunus necrotic ringspot virus. *J. Gen. Virol.* **85,** 761-768.

Hibi, T. and Furuki, I. (1985) Melon necrotic spot virus. In: *CMI/AAB Descriptions of Plant Viruses.* Warwick, UK: Association of Applied Biologists.

Hogle, J.M., Maeda, A. and Harrison, S.C. (1986) Structure and assembly of turnip crinkle virus. I. X-ray crystallographic structure analysis at 3.2 A resolution. *J. Mol. Biol.* **191,** 625-638.

Hsu, C., Singh, P., Ochoa, W., Manayani, D.J., Manchester, M., Schneemann, A. and Reddy, V. S. (2006) Characterization of polymorphism displayed by the coat protein mutants of tomato bushy stunt virus. *Virology,* **349,** 222-229.

Hui, E. and Rochon, D. (2006) Evaluation of the roles of specific regions of the Cucumber necrosis virus coat protein arm in particle accumulation and fungus transmission. *J. Virol.* **80,** 5968-5975.

Hui, E., Xiang, Y. and Rochon, D. (2010) Distinct regions at the N-terminus of the Cucumber necrosis virus coat protein target chloroplasts and mitochondria. *Virus Res.* **153,** 8-19.

Jansen, K.A., Wolfs, C.J., Lohuis, H., Goldbach, R.W. and Verduin, B.J. (1998) Characterization of the brome mosaic virus movement protein expressed in E. coli. *Virology,* **242,** 387-394.

Kakani, K., Reade, R., Katpally, U., Smith, T. and Rochon, D. (2008) Induction of particle polymorphism by cucumber necrosis virus coat protein mutants in vivo. *J. Virol.* **82,** 1547-1557.

Katpally, U., Kakani, K., Reade, R., Dryden, K., Rochon, D. and Smith, T.J. (2007) Structures of T=1 and T=3 particles of cucumber necrosis virus: evidence of internal scaffolding. *J. Mol. Biol.* **365,** 502-512.

Ke, J., Schmidt, T., Chase, E., Bozarth, R.F. and Smith, T.J. (2004) Structure of Cowpea mottle virus: a consensus in the genus Carmovirus. *Virology,* **321,** 349-358.

Knoester, M., van Loon, L.C., van den Heuvel, J., Hennig, J., Bol, J.F. and Linthorst, H.J. (1998) Ethylene-insensitive tobacco lacks nonhost resistance against soil-borne fungi. *Proc. Natl. Acad. Sci. U S A,* **95,** 1933-1937.

Kumar, A., Reddy, V.S., Yusibov, V., Chipman, P.R., Hata, Y., Fita, I., Fukuyama, K., Rossmann, M.G., Loesch-Fries, L.S., Baker, T.S. and Johnson, J.E. (1997) The structure of alfalfa mosaic virus capsid protein assembled as a T=1 icosahedral particle at 4.0-A resolution. *J. Virol.* **71,** 7911-7916.

Lacomme, C. and Chapman, S. (2008) Use of potato virus X (PVX)-based vectors for gene expression and virus-induced gene silencing (VIGS). *Curr Protoc Microbiol,* **Chapter 16,** Unit 16I 11.

Larson, S. B., Lucas, R. W. and McPherson, A. (2005) Crystallographic structure of the T=1 particle of brome mosaic virus. *J. Mol. Biol.* **346,** 815-831.

Marcos, J. F., Vilar, M., Pérez-Payá, E. and Pallás, V. (1999) In vivo detection, RNA-binding properties and characterization of the RNA-binding domain of the p7 putative movement protein from carnation mottle carmovirus (CarMV). *Virology,* **255,** 354-365.

Melnyk, C. W., Molnar, A. and Baulcombe, D.C. (2011) Intercellular and systemic movement of RNA silencing signals. *EMBO J.* **30,** 3553-3563.

Merai, Z., Kerenyi, Z., Kertesz, S., Magna, M., Lakatos, L. and Silhavy, D. (2006) Double-stranded RNA binding may be a general plant RNA viral strategy to suppress RNA silencing. *J. Virol.* **80,** 5747-5756.

Mochizuki, T., Ohnishi, J., Ohki, T., Kanda, A. and Tsuda, S. (2008) Amino acid substitution in the coat protein of Melon necrotic spot virus causes loss of binding to the surface of Olpidium bornovanus zoospores. *J. Gen. Plant Pathol.* **74,** 176-181.

Morgunova, E., Dauter, Z., Fry, E., Stuart, D. I., Stel'mashchuk, V., Mikhailov, A. M., Wilson, K.S. and Vainshtein, B.K. (1994) The atomic structure of Carnation Mottle Virus capsid protein. *FEBS Lett.* **338,** 267-271.

Navarro, J.A., Serra-Soriano, M. and Pallás, V. (2014) A protocol to measure the extent of cell-to-cell movement of RNA viruses in planta. *Bio-protocol,* **4,** e1269.

Ohki, T., Akita, F., Mochizuki, T., Kanda, A., Sasaya, T. and Tsuda, S. (2010) The protruding domain of the coat protein of Melon necrotic spot virus is involved in compatibility with and transmission by the fungal vector Olpidium bornovanus. *Virology,* **402,** 129-134.

Pallás, V., Mas, P. and Sánchez-Navarro, J.A. (1998) Detection of plant RNA viruses by nonisotopic dot-blot hybridization. *Methods Mol. Biol.* **81,** 461-468.

Pappachan, A., Subashchandrabose, C., Satheshkumar, P.S., Savithri, H.S. and Murthy, M.R. (2008) Structure of recombinant capsids formed by the beta-annulus deletion mutant -- rCP (Delta48-59) of Sesbania mosaic virus. *Virology,* **375,** 190-196.

Pérez-Cañamás, M. and Hernández, C. (2015) Key importance of small RNA binding for the activity of a glycine-tryptophan (GW) motif-containing viral suppressor of RNA silencing. *J. Biol. Chem.* **290,** 3106-3120.

Powers, J.G., Sit, T.L., Heinsohn, C., George, C.G., Kim, K.H. and Lommel, S.A. (2008) The Red clover necrotic mosaic virus RNA-2 encoded movement protein is a second suppressor of RNA silencing. *Virology,* **381,** 277-286.

Qu, F. and Morris, T.J. (1997) Encapsidation of turnip crinkle virus is defined by a specific packaging signal and RNA size. *J. Virol.* **71,** 1428-1435.

Rao, A.L. (2006) Genome packaging by spherical plant RNA viruses. *Annu. Rev. Phytopathol.* **44,** 61-87.

Reade, R., Kakani, K. and Rochon, D. (2010) A highly basic KGKKGK sequence in the RNA-binding domain of the Cucumber necrosis virus coat protein is associated with encapsidation of full-length CNV RNA during infection. *Virology,* **403,** 181-188.

Riviere, C.J., Pot, J., Tremaine, J.H. and Rochon, D.M. (1989) Coat protein of melon necrotic spot carmovirus is more similar to those of tombusviruses than those of carmoviruses. *J. Gen. Virol.* **70 (Pt 11),** 3033-3042.

Riviere, C.J. and Rochon, D.M. (1990) Nucleotide sequence and genomic organization of melon necrotic spot virus. *J. Gen. Virol.* **71,** 1887-1896.

Ryder, S.P., Recht, M.I. and Williamson, J.R. (2008) Quantitative analysis of protein-RNA interactions by gel mobility shift. *Methods Mol. Biol.* **488,** 99-115.

Sangita, V., Lokesh, G.L., Satheshkumar, P.S., Vijay, C.S., Saravanan, V., Savithri, H.S. and Murthy, M.R. (2004) T=1 capsid structures of Sesbania mosaic virus coat protein mutants: determinants of T=3 and T=1 capsid assembly. *J. Mol. Biol.* **342,** 987-999.

Satheshkumar, P.S., Lokesh, G.L., Murthy, M.R. and Savithri, H.S. (2005) The role of arginine-rich motif and beta-annulus in the assembly and stability of Sesbania mosaic virus capsids. *J. Mol. Biol.,* **353,** 447-458.

Serra-Soriano, M., Navarro, J.A., Genovés, A. and Pallás, V. (2015) Comparative proteomic analysis of melon phloem exudates in response to viral infection. *J. Proteomics,* **124,** 11-24.

Serra-Soriano, M., Pallás, V. and Navarro, J.A. (2014) A model for transport of a viral membrane protein through the early secretory pathway: minimal sequence and endoplasmic reticulum lateral mobility requirements. *Plant J.* **77,** 863-879.

Sherman, M.B., Guenther, R.H., Tama, F., Sit, T.L., Brooks, C.L., Mikhailov, A.M., Orlova, E.V., Baker, T.S. and Lommel, S.A. (2006) Removal of divalent cations induces structural transitions in red clover necrotic mosaic virus, revealing a potential mechanism for RNA release. *J. Virol.* **80,** 10395-10406.

Skuzeski, J.M. and Morris, T.J. (1995) Quantitative analysis of the binding of turnip crinkle virus coat protein to RNA fails to demonstrate binding specificity but reveals a highly cooperative assembly interaction. *Virology,* **210,** 82-90.

Timmins, P.A., Wild, D. and Witz, J. (1994) The three-dimensional distribution of RNA and protein in the interior of tomato bushy stunt virus: a neutron low-resolution single-crystal diffraction study. *Structure,* **2,** 1191-1201.

Voinnet, O., Pinto, Y.M. and Baulcombe, D.C. (1999) Suppression of gene silencing: a general strategy used by diverse DNA and RNA viruses of plants. *Proc. Natl. Acad. Sci. U S A,* **96,** 14147-14152.

Wada, Y., Tanaka, H., Yamashita, E., Kubo, C., Ichiki-Uehara, T., Nakazono-Nagaoka, E., Omura, T. and Tsukihara, T. (2008) The structure of melon necrotic spot virus determined at 2.8 A resolution. *Acta Crystallogr. Sect. F. Struct .Biol. Cryst. Commun.* **64,** 8-13.

Zhang, F. and Simon, A.E. (2003) Enhanced viral pathogenesis associated with a virulent mutant virus or a virulent satellite RNA correlates with reduced virion accumulation and abundance of free coat protein. *Virology,* **312,** 8-13.

SUPPORTING INFORMATION LEGENDS

Table S1. List of oligonucleotides used in this study

Fig. S1. Hill plots of RNA binding activity of GST-CP(wt) and GST recombinant R domain mutants.

Fig. S2. Amino acid sequence alignment of coat protein N-terminal regions of Melon necrotic spot virus (MNSV) and all available members of genus Tombusvirus.

FIGURE LEGENDS

Fig. 1. Linear order of the structural domains of MNSV CP (R, S and P) and location of R_1 (black lined boxes), R_2 (grey lined boxed) and R_3 (dark grey lined boxes) subdomains is shown at the top. The color code for secondary structure elements is as indicated. Amino acid sequence corresponds to the first 91 amino acids of R domain. Basic residues Lysine/Arginine are highlighted with the symbol “+”, and sequences corresponding to each R subdomain are colored according to the code assigned above. A schematic representation of MNSV CP R domain

mutants used in this study is shown below. Dashes correspond to deleted amino acids and, at the bottom, letters in bold within R_3 subdomain sequence correspond to positions changed in Ala substitution mutations. On the right, a ribbon drawing of C subunit of MNSV CP is displayed. In C type subunit, R_3 subdomain was comprised of a β annular structure and a downstream sequence termed "ε" region. Spatial distribution of side chains of basic residues mutated within R_3 subdomain is shown. Secondary structure elements of S and P domains are indicated by twisted (α-helix) and arrowed (β-strand) ribbons.

Fig. 2. Analysis of RNA binding activity of MNSV CP and R domain mutants by EMSA. Complexes were hardly transferred to membranes since they barely enter the gel; therefore, only disappearance of unbound RNA from representative EMSAs is shown. The apparent dissociation constant calculated using a Hill transformation of data is showed on the right of the corresponding shift gel.

Fig. 3. Effects of MNSV CP R domain mutations on viral RNA encapsidation. (A) Schematic diagram of the MNSV genome organization. (B) Dot-blot immunodetection of viral particles produced by the indicated MNSV CP R domain mutants. Virions were purified through a 20% sucrose and serial dilutions applied to a PVDF membrane. (C) Northern blot analysis of MNSV RNAs associated to virions produced by MNSV CP R domain mutants. Loaded samples were adjusted to have approximately equal amounts of virions as revealed by the dot-blot immunodetection included below. (D) Denaturing agarose gel electrophoresis and Northern blot of total RNA isolated from cotyledon extracts infected with the indicated mutants. Position of MNSV genomic and both subgenomic RNAs is indicated. E) Northern blot analysis of RNAs isolated from purified virions produced by CP($\Delta R_{1,2}$), CP(ΔR_2), CP(ΔR_1), CP(R81A) and CP(wt). Position of a putative defective interfering RNA (DI RNA) is indicated.

Fig. 4. Influence of mutations in MNSV CP R domain on viral cell-to-cell movement in *C. melo*. A) Schematic representation of recombinant MNSV(AI)/GFP genome cloned into pMOG800 under the control of the CaMV 35S promoter. eGFP and CP were simultaneously expressed using the 'self-cleaving' TAV 2a peptide. Viral and fluorescent protein names are indicated. (B)

Quantification of cell-to-cell movement of wild-type MNSV(AI)/GFP and CP R domain mutants. Recombinant binary vectors were agroinfiltrated into *C. melo* leaves and, after imaging, fluorescent areas corresponding to infection foci were measured at 6 and 12 days post-infiltration. The results are presented as the average of infection foci size means from three separated experiments. (C) Representative images of fluorescent infection foci produced by wild-type MNSV(AI)/GFP and indicated CP R domain mutants at 12 days post-inoculation. Infiltration of bacteria carrying empty pMOG800 was used as negative control for autofluorescence.

Fig. 5. Increasing of PVX pathogenicity and viral RNA accumulation is facilitated by MNSV CP R domain. (A) Symptoms of infection with "empty" PVX or PVX expressing MNSV CP (wild-type or the indicated mutants) in *N. benthamiana* plants. Images were taken three weeks after agroinfiltration. (B) Northern blot analysis with PVX CP specific riboprobe of total RNAs of representative *N. benthamiana* plants systemically infected with "empty" PVX or PVX expressing MNSV CP (wild-type or the indicated mutants). Healthy control plants were agroinfitrated with bacteria carrying empty pMOG800.

Fig. 6. Analysis of small RNA (sRNA) binding activity of MNSV CP(wt) by EMSA. (A) Gel retardation assays of single stranded viral transcripts (ssRNAs) of 21, 22 or 24 nt with GST-CP(wt). Bands corresponding to unbound sRNA were quantified to calculate the apparent dissociation constant. (B). Hill plots of sRNA binding activity of GST-CP(wt). A Hill transformation was applied to data to graphically represent the log [(1-x)/x] versus the log[CP], were x is the ratio of unbound RNA to total RNA. Lines represent the best fit determined by least square analysis of the mean values from at least three separated experiments. The corresponding equation and R-squared value are given in each graph.

Fig. 7. Comparison of small RNA (sRNA) binding activity of MNSV CP(wt) and R domain mutants by EMSA. Single stranded RNAs (ssRNA) of 21, 22, or 24 nt (A) and the corresponding RNAs duplexes (dsRNA) containing 2-nt 3' end overhangs (B) were incubated with 600 nM of GST-CP(wt) or the indicated GST-recombinant R domain mutants. No protein was included in the control mix.

Fig. 8. Effects of MNSV CP and R domain mutants on systemic GFP silencing. At the 4 leaf stage, GFP transgenic *N. benthamiana* plants (line 16c) were coinfiltrated with agrobacteria expressing eGFP plus MNSV CP wild type and the indicated mutants. 25-30 days later, photographs were taken under long-wavelength UV light.

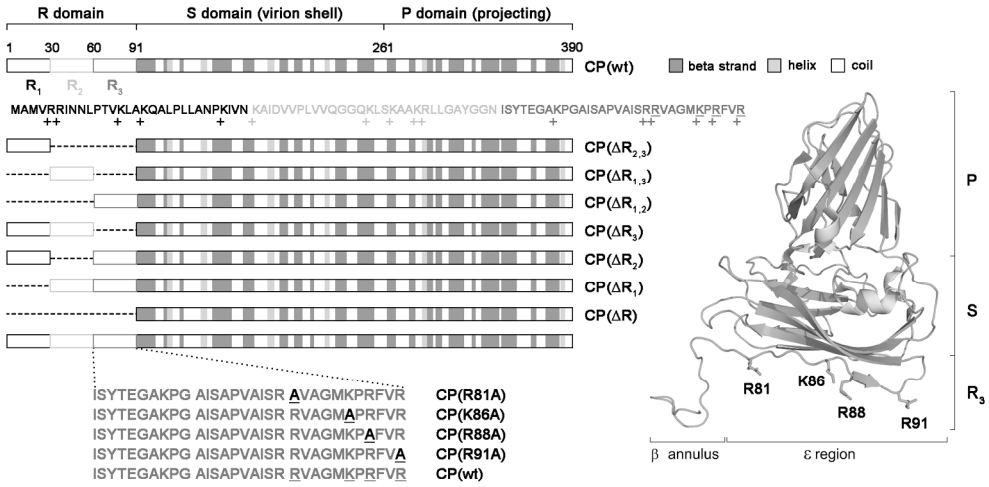

Figure 1

Fig. 1. Linear order of the structural domains of MNSV CP (R, S and P) and location of R1 (black lined boxes), R2 (grey lined boxed) and R3 (dark grey lined boxes) subdomains is shown at the top. The color code for secondary structure elements is as indicated. Amino acid sequence corresponds to the first 91 amino acids of R domain. Basic residues Lysine/Arginine are highlighted with the symbol "+", and sequences corresponding to each R subdomain are colored according to the code assigned above. A schematic representation of MNSV CP R domain mutants used in this study is shown below. Dashes correspond to deleted amino acids and, at the bottom, letters in bold within R3 subdomain sequence correspond to positions changed in Ala substitution mutations. On the right, a ribbon drawing of C subunit of MNSV CP is displayed. In C type subunit, R3 subdomain was comprised of a β annular structure and a downstream sequence termed "ε" region. Spatial distribution of side chains of basic residues mutated within R3 subdomain is shown. Secondary structure elements of S and P domains are indicated by twisted (α-helix) and arrowed (β-strand) ribbons.
168x99mm (300 x 300 DPI)

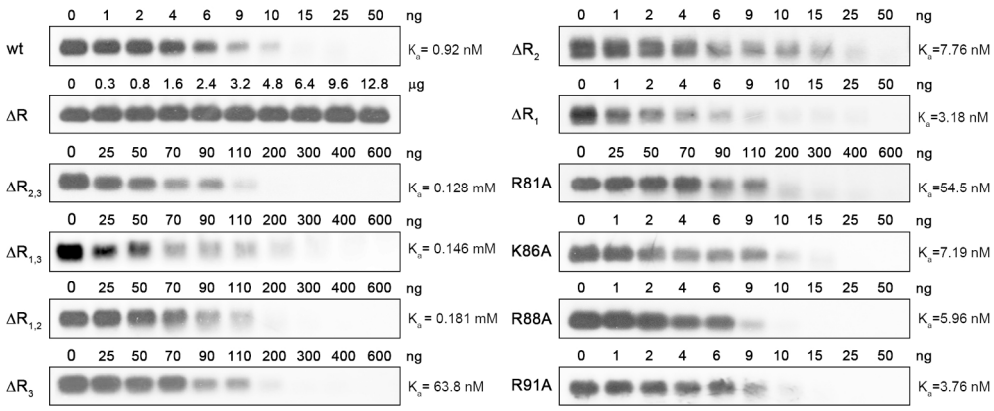

Figure 2

Fig. 2. Analysis of RNA binding activity of MNSV CP and R domain mutants by EMSA. Complexes were hardly transferred to membranes since they barely enter the gel; therefore, only disappearance of unbound RNA from representative EMSAs is shown. The apparent dissociation constant calculated using a Hill transformation of data is showed on the right of the corresponding shift gel.

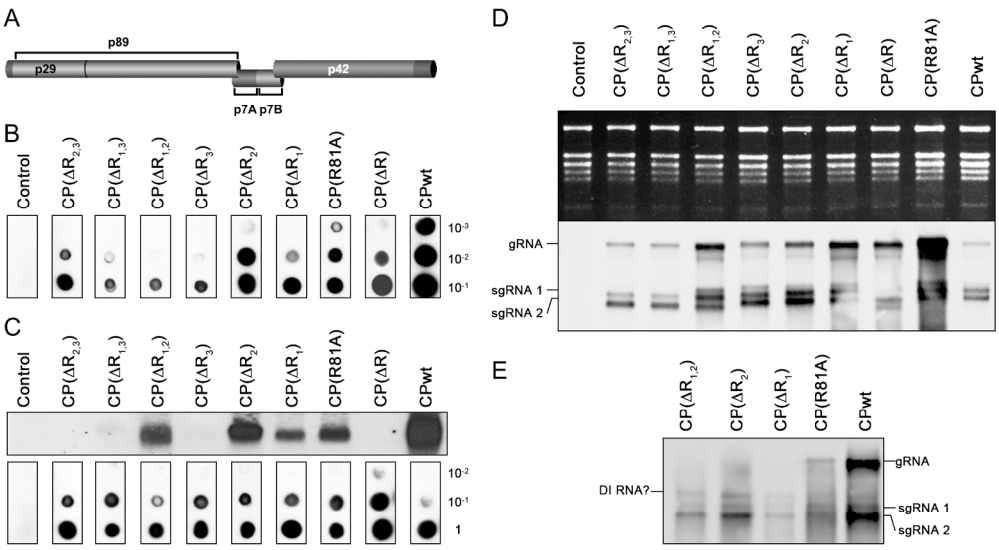

Figure 3

Fig. 3. Effects of MNSV CP R domain mutations on viral RNA encapsidation. (A) Schematic diagram of the MNSV genome organization. (B) Dot-blot immunodetection of viral particles produced by the indicated MNSV CP R domain mutants. Virions were purified through a 20% sucrose and serial dilutions applied to a PVDF membrane. (C) Northern blot analysis of MNSV RNAs associated to virions produced by MNSV CP R domain mutants. Loaded samples were adjusted to have approximately equal amounts of virions as revealed by the dot-blot immunodetection included below. (D) Denaturing agarose gel electrophoresis and Northern blot of total RNA isolated from cotyledon extracts infected with the indicated mutants. Position of MNSV genomic and both subgenomic RNAs is indicated. E) Northern blot analysis of RNAs isolated from purified virions produced by CP(ΔR1,2), CP(ΔR2), CP(ΔR1), CP(R81A) and CP(wt). Position of a putative defective interfering RNA (DI RNA) is indicated.
171x104mm (300 x 300 DPI)

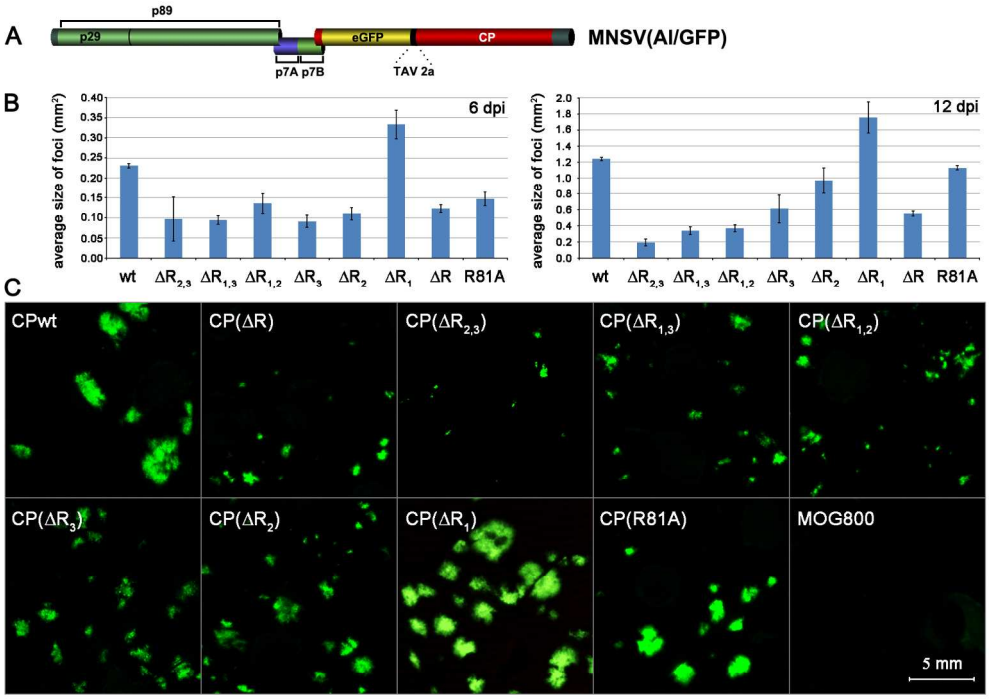

Figure 4

Fig. 4. Influence of mutations in MNSV CP R domain on viral cell-to-cell movement in C. melo. A) Schematic representation of recombinant MNSV(AI)/GFP genome cloned into pMOG800 under the control of the CaMV 35S promoter. eGFP and CP were simultaneously expressed using the 'self-cleaving' TAV 2a peptide. Viral and fluorescent protein names are indicated. (B) Quantification of cell-to-cell movement of wild-type MNSV(AI)/GFP and CP R domain mutants. Recombinant binary vectors were agroinfiltrated into C. melo leaves and, after imaging, fluorescent areas corresponding to infection foci were measured at 6 and 12 days post-infiltration. The results are presented as the average of infection foci size means from three separated experiments. (C) Representative images of fluorescent infection foci produced by wild-type MNSV(AI)/GFP and indicated CP R domain mutants at 12 days post-inoculation. Infiltration of bacteria carrying empty pMOG800 was used as negative control for autofluorescence.
175x135mm (299 x 299 DPI)

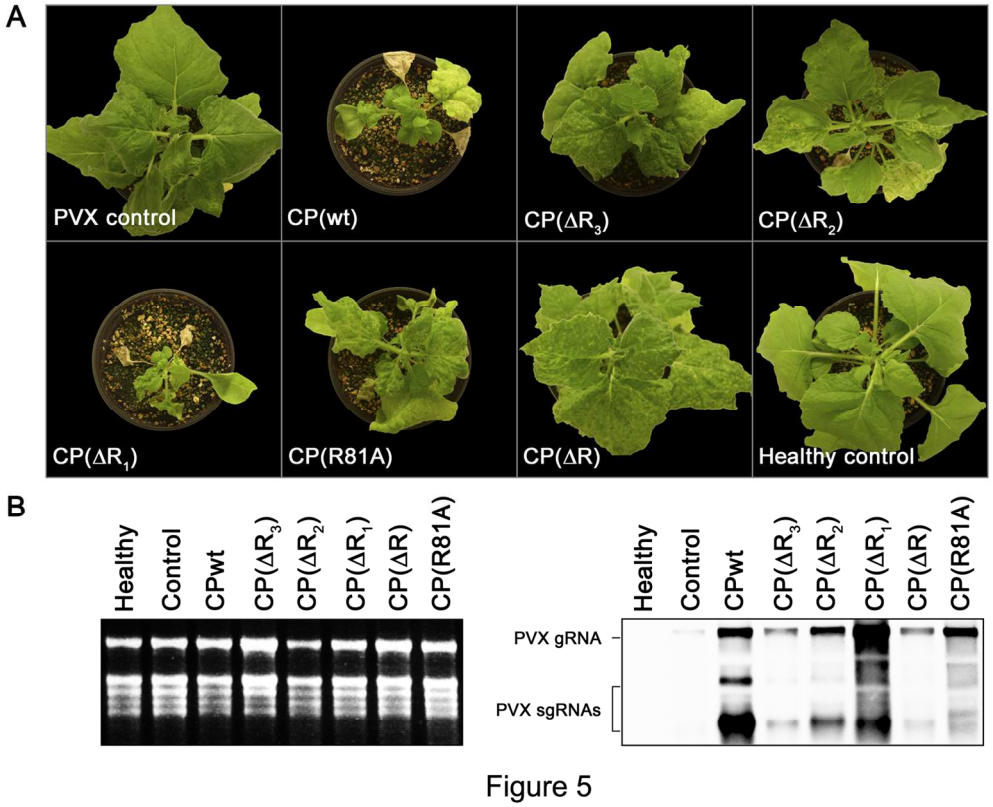

Figure 5

Fig. 5. Increasing of PVX pathogenicity and viral RNA accumulation is facilitated by MNSV CP R domain. (A) Symptoms of infection with "empty" PVX or PVX expressing MNSV CP (wild-type or the indicated mutants) in N. benthamiana plants. Images were taken three weeks after agroinfiltration. (B) Northern blot analysis with PVX CP specific riboprobe of total RNAs of representative N. benthamiana plants systemically infected with "empty" PVX or PVX expressing MNSV CP (wild-type or the indicated mutants). Healthy control plants were agroinfitrated with bacteria carrying empty pMOG800.
145x119mm (300 x 300 DPI)

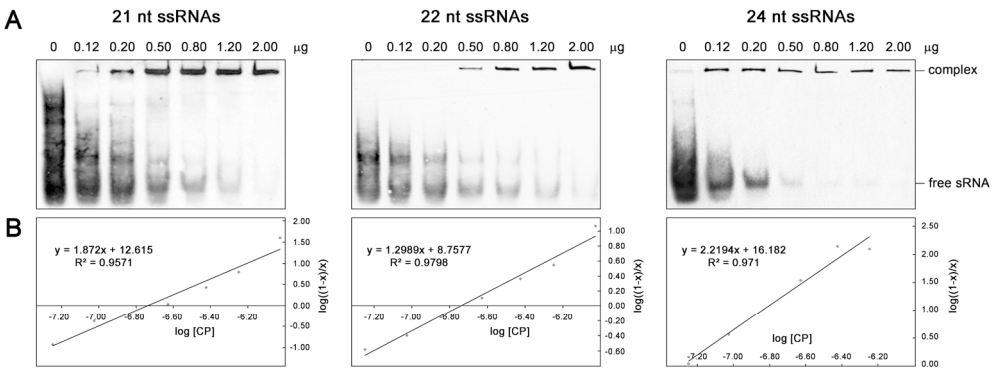

Figure 6

Fig. 6. Analysis of small RNA (sRNA) binding activity of MNSV CP(wt) by EMSA. (A) Gel retardation assays of single stranded viral transcripts (ssRNAs) of 21, 22 or 24 nt with GST-CP(wt). Bands corresponding to unbound sRNA were quantified to calculate the apparent dissociation constant. (B). Hill plots of sRNA binding activity of GST-CP(wt). A Hill transformation was applied to data to graphically represent the log [(1-x)/x] versus the log[CP], were x is the ratio of unbound RNA to total RNA. Lines represent the best fit determined by least square analysis of the mean values from at least three separated experiments. The corresponding equation and R-squared value are given in each graph.
168x70mm (300 x 300 DPI)

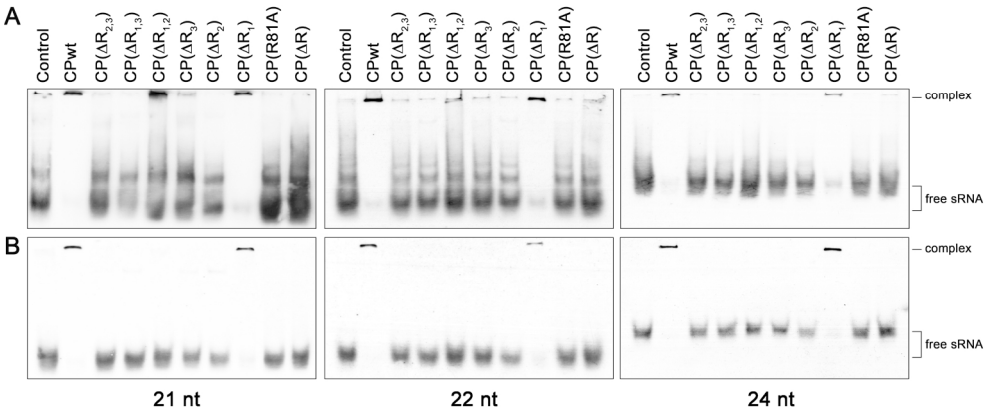

Figure 7

Fig. 7. Comparison of small RNA (sRNA) binding activity of MNSV CP(wt) and R domain mutants by EMSA. Single stranded RNAs (ssRNA) of 21, 22, or 24 nt (A) and the corresponding RNAs duplexes (dsRNA) containing 2-nt 3′ end overhangs (B) were incubated with 600 nM of GST-CP(wt) or the indicated GST-recombinant R domain mutants. No protein was included in the control mix.
177x85mm (300 x 300 DPI)

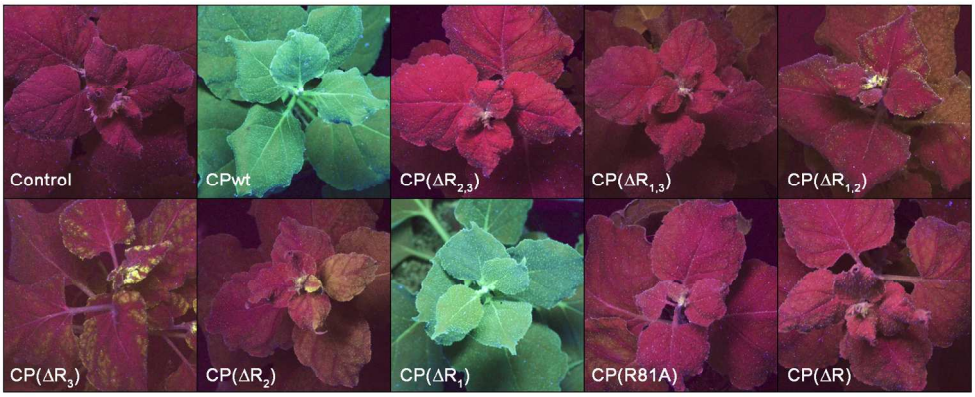

Figure 8

Fig. 8. Effects of MNSV CP and R domain mutants on systemic GFP silencing. At the 4 leaf stage, GFP transgenic N. benthamiana plants (line 16c) were coinfiltrated with agrobacteria expressing eGFP plus MNSV CP wild type and the indicated mutants. 25-30 days later, photographs were taken under long-wavelength UV light.
177x85mm (299 x 299 DPI)